Conf-951135--9
SAND95-1376C

RESISTOR CAPACITOR, PRIMITIVE VARIABLE SOLUTION OF BUOYANT FLUID FLOW WITHIN AN ENCLOSURE WITH HIGHLY TEMPERATURE DEPENDENT VISCOSITY

Shawn P. Burns
The University of Texas at Austin
Austin, TX

Steven E. Gianoulakis
Sandia National Laboratories
Albuquerque, NM

ABSTRACT

A numerical solution for buoyant natural convection within a square enclosure containing a fluid with highly temperature dependent viscosity is presented. Although the fluid properties employed do not represent any real fluid, the large variation in the fluid viscosity with temperature is characteristic of turbulent flow modeling with eddy-viscosity concepts. Results are obtained using a primitive variable formulation and the resistor capacitor method. The results presented include velocity, temperature and pressure distributions within the enclosure as well as shear stress and heat flux distributions along the enclosure walls. Three mesh refinements were employed and uncertainty values are suggested for the final mesh refinement. These solutions are part of a contributed benchmark solution set. for the subject problem

NOMENCLATURE

General

$\mathbf{u}$	Dimensionless velocity vector, $\mathbf{u}= u\mathbf{i} + v\mathbf{j}$
P	Dimensionless pressure
P	Characteristic pressure
f	Dimensionless absolute viscosity, $f= \mu(T)/\mu_o$
g	Acceleration due to gravity
L	Enclosure side length
N	Number of nodes in the mesh
q'	Linear heat rate
Ra_o	Rayleigh number (Eq.(5))
Pr_o	Prandtl number, $Pr_o= \nu(T_o)/\alpha$

This work was supported by the United States Department of Energy under Contract DE-AC04-94AL85000.

DISCLAIMER

T^*	Temperature
ΔT	Enclosure temperature drop, $\Delta T = T_H - T_C$
U	Characteristic velocity
$\mathbf{x}$	Dimensionless position vector, $\mathbf{x} = x\mathbf{i} + y\mathbf{j}$

Greek

α	Thermal diffusivity
β	Volumetric thermal expansion coefficient
ε_q	Heat balance error (Eq.(7))
T	Dimensionless temperature, $T = (T^* - T_o)/\Delta T$
μ	Absolute viscosity
ν	Dynamic viscosity
$\partial\Omega$	Enclosure boundary

Subscript

max	Maximum nodal quantity
min	Minimum nodal quantity
o	Indicates evaluation at the mean enclosure temperature, $T_o = (T_H + T_C)/2$
H	Hot wall, x/L= 0
C	Cold wall, x/L= 1

PROBLEM DESCRIPTION

The problem geometry consists of a square enclosure of side length L, $x \in [0, L]$, $y \in [0, L]$ with the left wall maintained at a higher temperature than the right wall, $T(0, y) = T_H > T_C = T(L, y)$. The horizontal walls are insulated and gravity is directed in the -y direction. With the exception of the density and viscosity, all of the material properties are assumed to be constant. The variation of the fluid density with temperature is modeled using the Oberbeck-Boussinesq approximation [Patankar, 1980]. The viscosity variation is given by:

$$\frac{\mu(T)}{\mu_o} = f\left(\frac{T}{T_o}\right) = \begin{cases} 0.900\dfrac{T}{T_o} + 0.470, & -0.5 \le \dfrac{T}{T_o} < -0.3 \\ 2.67\dfrac{T}{T_o} + 1.00, & -0.3 \le \dfrac{T}{T_o} < 0.3 \\ 91.0\dfrac{T}{T_o} - 25.5, & 0.3 \le \dfrac{T}{T_o} \le 0.5 \end{cases} \qquad (1)$$

where T_o is the mean enclosure temperature, $T_o = (T_H + T_C)/2$. The fluid Prandtl number was evaluated at the mean enclosure temperature and is $Pr_o = 0.71$ for all of the results presented here. This problem was formulated by an external source to be a benchmark problem examining various contributed solution procedures.

Assumptions

1) Low speed flow
2) Two dimensional flow
3) Steady flow
4) Constant specific heat, thermal conductivity
5) Oberbeck-Boussinesq approximation for density

GOVERNING EQUATIONS

The following list summarizes the characteristic values used to scale the governing transport equations for mass, momentum and energy:

Characteristic length - L

Characteristic velocity - $U = \sqrt{g\beta\Delta TL}$

Characteristic pressure - $P = \mu(T_o)U_o/L$

Characteristic temperature drop - $\Delta T = T_H - T_C$

Given the assumptions discussed in the problem description, the scaled transport equations for mass, momentum, and energy may then be written:

$$\nabla \cdot \boldsymbol{u} = 0 \tag{2}$$

$$\sqrt{\frac{Ra_o}{Pr_o}}\boldsymbol{u}\cdot\nabla\boldsymbol{u} = -\nabla P + \nabla\cdot\left[f(\theta)\nabla\boldsymbol{u}\right] + \sqrt{\frac{Ra_o}{Pr_o}}\theta\hat{\boldsymbol{j}} \tag{3}$$

$$\sqrt{Ra_o Pr_o}\,\boldsymbol{u}\cdot\nabla\theta = \nabla^2\theta \tag{4}$$

where the Rayleigh number is given by:

$$Ra_o = \frac{g\beta\Delta TL^3}{\nu_o\alpha} \tag{5}$$

Boundary Conditions

The follwing boundary conditions were used as specfied in the provided problem statement:

$$\theta(0,y) = 0.5 \ \forall \ y \in [0,1] \tag{6}$$

$$\theta(1,y) = -0.5 \ \forall \ y \in [0,1] \tag{7}$$

$$\frac{\partial \theta}{\partial y}(x,0) = \frac{\partial \theta}{\partial y}(x,1) = 0.0 \ \forall \ x \in (0,1) \tag{8}$$

$$u(x,y) = v(x,y) = 0 \ \forall \ (x,y) \in \partial\Omega \tag{9}$$

SOLUTION METHOD

Equations (2)-(4) are evaluated using a resistor capacitor solution method similar to that described by Patankar (1980) using collocated velocity and pressure nodes. A collocated version of Patankar's SIMPLER algorithm was developed in the thesis by Burns (1990) and was later employed in the TEXSAN thermal-hydraulic analysis program (Burns and Klein, 1993). The TEXSAN program employs a translation method described in the dissertation by Gianoulakis (1992) to extract resistor capacitor information from a finite element mesh. Bilinear (4-node quadrilateral) elements were employed to obtain all of the results presented in this work. Figure 1 shows a typical resistor capacitor computational molecule which arises from the TEXSAN translation method using a mesh of bilinear elements.

The TEXSAN program employs a Picard iteration method to evaluate the temperature, pressure, and velocity components at each of the nodes in the mesh. Iterations continued until the following condition was met:

$$\frac{\left|\phi_i^n - \phi_i^{n-1}\right|}{\phi_{max} - \phi_{min}} < 10^{-6} \ \forall \ i \in [1, N] \ \wedge \ \phi \in \{u, v, T, P\} \tag{10}$$

where n represents the current iteration level and n-1 represents the previous iteration level.

COMPUTATIONAL DETAILS

To assess the solution accuracy, the linear heat rates at the hot and cold walls were compared and the following heat balance error defined

$$\varepsilon_q = \frac{\left|q'(x=0) - q'(x=1)\right|}{\overline{q'}} \tag{11}$$

The mesh spacing was refined until the heat balance error for all values of the Rayleigh number was less than 1-2%. A 60×60 element grid with 8:1 node refinement at the wall met this criteria. The refinement ratio represents the ratio of the node spacing at the center of the enclosure to the normal node spacing directly adjacent to any wall. The results from the 60×60, 8:1 mesh were then compared to results using an 80×80 mesh with 8:1 mesh refinement at the walls to check mesh independence. The relative change in the results from the 60×60, 8:1 mesh and the 80×80, 8:1 mesh are summarized in the principal results section.

All tabulated values presented in the proceeding sections represent nodal values with no interpolation between nodal locations. The shear stress and Nusselt numbers were calculated using a quadratic curve fit of the wall node and its two nearest neighbors along a line perpendicular to the wall. It will be shown that the postprocessing method used to determine the wall shear stress from the nodal velocities may have a dramatic effect on the final shear stress value. Linear interpolation between nodal values was used in some of the profiles in Figures 2-13 to provide the profiles at x and y= 0.05. The construction of the finite element mesh assured that nodes always lay on the boundaries as well as along the enclosure centerlines.

VERIFICATION

de Vahl Davis and Jones (1983) and de Vahl Davis (1983) present a bench mark numerical solution for buoyant fluid flow and heat transfer within a square enclosure with constant fluid properties and a Prandtl number of 0.71. This section compares the current TEXSAN solution using a uniform 60×60 mesh with the previous results provided by de Vahl Davis (1983). A more limited comparison between the TEXSAN program and the de Vahl Davis results is also provided by Burns and Klein (1993) using a uniform mesh of three noded triangular elements.

Table 1 compares the TEXSAN solution with the de Vahl Davis bench mark solution for all three values of the Rayleigh number considered. The quantities shown in Table 1 are defined by de Vahl Davis and Jones (1983) and represent values along the horizontal and vertical centerlines and the hot wall of the enclosure. The heat balance error (Eq.(11)) for the TEXSAN results shown in Table 1 are 1.01% for $Ra_o = 10^4$, 1.10% for $Ra_o = 10^5$, and 1.26% for $Ra_o = 10^6$.

PRINCIPAL RESULTS

Tables 2-13 and Figures 2-13 summarize the principal numerical results obtained using the 80×80, 8:1 mesh described above. The heat balance error (Eq.(11)) corresponding to the 80×80, 8:1 mesh results are 0.28% for $Ra_o = 10^4$, 0.05% for $Ra_o = 10^5$, and 0.62% for $Ra_o = 10^6$. The tables include data from a uniform 40×40 mesh as well as the 60×60, 8:1 mesh and 80×80, 8:1 mesh. Tables 14-16 provide data relating to the computational effort required to obtain the solutions presented here for each mesh and at each Rayleigh number. All of the results were obtained using a CRAY Y-MP8/864 supercomputer running the UNICOS operating system version 8.0.3.1

To provide some measure of the solution accuracy, the maximum changes in the data shown in Tables 2-13 for the 60×60, 8:1 and 80×80, 8:1 mesh results were calculated. The shear stress values showed the greatest variation between the two mesh spacings. The *maximum* shear stress value changed by as much as 11.6% of the 80×80, 8:1 mesh results and the greatest change in the position of the maximum shear stress was 5.7% of the enclosure width, L. The change in the maximum shear stress is much smaller along walls where the velocity gradients are smaller. From Table 4, the change in the maximum shear stress value between the 60×60, 8:1 and the 80×80, 8:1 mesh was less than 2.4% of the 80×80, 8:1 mesh value along the hot wall.

Since the *minimum* shear stress values were very close to zero, the relative change in these values was typically very large. The position of the minimum shear stress values, however, changed by less than 2.4% of L between the 60×60, 8:1 and the 80×80, 8:1 mesh results.

The variation of the Nusselt number values between the 60×60, 8:1 and 80×80, 8:1 mesh results was in general much better than the shear stress values. The *maximum* Nusselt number changed by less than 1.2% of the 80×80, 8:1 mesh value between the two mesh spacings and the position of the maximum changed by less than 1.2% of L. The change in the *minimum* Nusselt number values was less than 3.6% of the 80×80, 8:1 mesh value and the position of the minimum changed by less than 0.5% of L.

The maximum centerline velocity components shown in Tables 2 and 11 changed by less that 6.8% of the 80×80, 8:1 mesh value between the 60×60, 8:1 and the 80×80, 8:1 mesh results. The corresponding change in the position of the maximum centerline velocity components was less than 0.96% of L. The u velocity component along the vertical centerline showed a larger variation between the two mesh spacings than did the v component along the horizontal centerline. The greatest change in the maximum v velocity component along the horizontal centerline was less than 2.0% of the 80×80, 8:1 mesh value.

A two point approximation was also employed to calculate the temperature and velocity gradients at the walls. When compared to the three point approximation used to obtain the values in Tables 3-10, 12-13, it was found that the maximum shear stress values changed by as much as 27% of the three point values when a two point approximation was employed. The locations of the maximum shear stresses also changed by as much as 7.1% of L when a two point approximation was employed.

The effect of the postprocessing method was much less pronounced when calculating the Nusselt number values. The maximum Nusselt number value changed by less than 1.2% of the values shown in Tables 8 and 10 when a two point approximation was used for the wall temperature gradient. The corresponding change in the minimum Nusselt number values was less than 0.22% of the values shown in Tables 7 and 9. The positions of the extreme Nusselt number values changed by less than 0.54% of L when a two point approximation was employed.

Convergence was not smooth for the highest Rayleigh number, $Ra_o = 10^6$, for both the 60×60, 8:1 and the 80×80, 8:1 meshes. Reasonably smooth convergence was obtained for $Ra_o = 10^4$, and 10^6 using an underrelaxation coefficient of 0.5 for both the temperature and velocity systems. For $Ra_o = 10^6$, however, it was necessary to decrease the underrelaxation coefficient to 0.2 to obtain a convergence level of $O(10^{-5} - 10^{-6})$ (cf. Eq.(6)) for the 60×60, 8:1 and the 80×80, 8:1 meshes. The computation time shown in Table 16 reflects the slower convergence rate brought about by the smaller underrelaxation level.

CONCLUSIONS

A numerical solution for buoyant natural convection within an enclosure containing a fluid with highly temperature dependent viscosity is presented. The numerical results presented were obtained from a resistor capacitor network constructed from a mesh of 80×80 bilinear finite elements with an 8:1 mesh refinement at the enclosure walls. The solution presented is intended to contribute to a bench mark solution set for the problem described. This problem was developed by an source other than the authors.

Based upon mesh refinement data, the current solution involves an uncertainty in the local velocities of approximately 7% of the maximum velocity. The local Nusselt numbers are known to within 1-4% of the local value and the local shear stress to within 12% of the maximum shear stress value. Along walls with small velocity gradients, the shear stress uncertainty decreases to on the order of 2% of the maximum value.

The shear stress values presented should be approached with some caution as they are very sensitive to the postprocessing method employed. It was shown that the use of a two

point or three point approximation to the velocity gradient at the walls could result in as high as a 27% change in the maximum wall shear stress values.

REFERENCES

S.P.Burns, 1990, A Collocated Control Volume Finite Difference Method for High Level Nuclear Waste Shipping Cask Analysis, Masters Thesis, The University of Texas at Austin, Austin, TX, August

S.P.Burns, D.E.Klein, 1993, "Validation of the TEXSAN Thermal-Hydraulic Analysis Program", Nuclear Technology, vol. 104, November, pp. 157-163

G. de Vahl Davis, I.P. Jones, 1983, "Natural Convection in a Square Cavity: A Comparison Exercise", International Journal for Numerical Methods in Fluids, vol.3, pp. 227-248

G. de Vahl Davis, 1983, "Natural Convection of Air in a Square Cavity: A Bench Mark Numerical Solution", International Journal for Numerical Methods in Fluids, vol.3, pp. 249-264

S.E.Gianoulakis, A Hybrid Finite Element Finite Difference Method for Multi-Mode Heat Transfer in Complex Geometries, Ph.D. Dissertation, The University of Texas at Austin, Austin, TX, May

S.V.Patankar, 1980, Numerical Heat Transfer and Fluid Flow, Hemisphere Publishing Corp., New York, NY

TABLE 1 Comparison of TEXSAN Solution to Bench Mark Solution for Constant Viscosity

	$Ra_o = 10^4$		$Ra_o = 10^5$		$Ra_o = 10^6$	
Value	TEXSAN	1983[1]	TEXSAN	1983[1]	TEXSAN	1983[1]
$u_{max}(x = 0.5)$	0.191	0.192	0.137	0.130	0.0837	0.0767
y	0.817	0.823	0.850	0.855	0.850	0.850
$v_{max}(y = 0.5)$	0.228	0.233	0.251	0.257	0.249	0.260
x	0.117	0.119	0.067	0.066	0.0500	0.0379
$\overline{Nu}\ (x = 0)$	2.264	2.238	4.687	4.509	9.304	8.817
$Nu_{max}(x=0)$	3.539	3.528	7.765	7.717	17.767	17.925
y	0.150	0.143	0.100	0.081	0.0500	0.0378

[1] - Bench Mark Solution from G. de Vahl Davis, 1983

TABLE 2 - Maximum Nodal u Velocity Component Along (0.5, y)

	$Ra_o = 10^4$		$Ra_o = 10^5$		$Ra_o = 10^6$	
Mesh	u_{max}	y	u_{max}	y	u_{max}	y
40×40, 1:1	-0.288	0.100	-0.209	0.100	-0.124	0.100
60×60, 8:1	-0.342	0.0898	-0.306	0.0690	-0.260	0.0510
80×80, 8:1	-0.349	0.0905	-0.318	0.0672	-0.279	0.0414

TABLE 3 - Minimum Nodal Shear Stress Along (0.0, y), $y \in (0, 1)$

	$Ra_o = 10^4$		$Ra_o = 10^5$		$Ra_o = 10^6$	
Mesh	$\partial u/\partial x\|_{min}$	y	$\partial u/\partial x\|_{min}$	y	$\partial u/\partial x\|_{min}$	y
40×40, 1:1	0.0448	0.975	0.153	0.975	0.489	0.975
60×60, 8:1	2.64×10^{-3}	0.978	0.0144	0.990	0.0633	0.990
80×80, 8:1	1.04×10^{-3}	0.980	9.72×10^{-3}	0.984	0.0432	0.992

TABLE 4 - Maximum Nodal Shear Stress Along (0.0, y)

	$Ra_o = 10^4$		$Ra_o = 10^5$		$Ra_o = 10^6$	
Mesh	$\partial u/\partial x\|_{max}$	y	$\partial u/\partial x\|_{max}$	y	$\partial u/\partial x\|_{max}$	y
40×40, 1:1	0.486	0.425	0.680	0.375	1.28	0.125
60×60, 8:1	0.535	0.359	0.982	0.302	1.63	0.330
80×80, 8:1	0.538	0.367	0.988	0.323	1.67	0.303

TABLE 5 - Minimum Nodal Shear Stress Along (1.0, y)

Mesh	$Ra_o = 10^4$		$Ra_o = 10^5$		$Ra_o = 10^6$	
	$\partial u/\partial x\|_{min}$	y	$\partial u/\partial x\|_{min}$	y	$\partial u/\partial x\|_{min}$	y
40×40, 1:1	0.567	0.975	-0.184	0.0500	2.67	0.0500
60×60, 8:1	-0.361	0.990	0.164	0.990	-1.823	0.0510
80×80, 8:1	0.293	0.988	0.135	0.992	1.586	0.0746

TABLE 6 - Maximum Nodal Shear Stress Along (1.0, y)

Mesh	$Ra_o = 10^4$		$Ra_o = 10^5$		$Ra_o = 10^6$	
	$\partial u/\partial x\|_{max}$	y	$\partial u/\partial x\|_{max}$	y	$\partial u/\partial x\|_{max}$	y
40×40, 1:1	16.9	0.525	16.6	0.525	153	0.575
60×60, 8:1	49.2	0.539	73.9	0.424	102	0.359
80×80, 8:1	52.4	0.530	81.4	0.471	115	0.416

TABLE 7 - Minimum Nodal Nusselt Number Along (0.0, y)

Mesh	$Ra_o = 10^4$		$Ra_o = 10^5$		$Ra_o = 10^6$	
	$-\partial\theta/\partial x\|_{min}$	y	$-\partial\theta/\partial x\|_{min}$	y	$-\partial\theta/\partial x\|_{min}$	y
40×40, 1:1	0.921	0.975	1.28	0.975	2.13	0.950
60×60, 8:1	0.928	1.00	1.23	0.995	1.75	0.995
80×80, 8:1	0.920	1.00	1.21	1.00	1.69	0.996

TABLE 8 - Maximum Nodal Nusselt Number Along (0.0, y)

Mesh	$Ra_o = 10^4$		$Ra_o = 10^5$		$Ra_o = 10^6$	
	$-\partial\theta/\partial x\|_{max}$	y	$-\partial\theta/\partial x\|_{max}$	y	$-\partial\theta/\partial x\|_{max}$	y
40×40, 1:1	3.40	0.125	6.90	0.075	16.5	0.00
60×60, 8:1	3.57	0.127	7.29	0.127	14.5	0.0354
80×80, 8:1	3.58	0.128	7.26	0.139	14.1	0.0358

TABLE 9 - Minimum Nodal Nusselt Number Along (1.0, y)

Mesh	$Ra_o = 10^4$		$Ra_o = 10^5$		$Ra_o = 10^6$	
	$-\partial\theta/\partial x\|_{min}$	y	$-\partial\theta/\partial x\|_{min}$	y	$-\partial\theta/\partial x\|_{min}$	y
40×40, 1:1	0.458	0.00	0.703	0.00	1.80	0.000
60×60, 8:1	0.467	0.00	0.678	0.00	0.985	0.000
80×80, 8:1	0.464	0.00	0.678	0.00	1.00	0.000

TABLE 10 - Maximum Nodal Nusselt Number Along (1.0, y)

	$Ra_o = 10^4$		$Ra_o = 10^5$		$Ra_o = 10^6$	
Mesh	$-\partial\theta/\partial x\|_{max}$	y	$-\partial\theta/\partial x\|_{max}$	y	$-\partial\theta/\partial x\|_{max}$	y
40×40, 1:1	3.39	0.850	6.82	0.925	14.2	0.950
60×60, 8:1	3.57	0.843	7.46	0.910	16.5	0.957
80×80, 8:1	3.57	0.838	7.52	0.918	16.7	0.959

TABLE 11 - Maximum Nodal v Velocity Component Along (x, 0.5)

	$Ra_o = 10^4$		$Ra_o = 10^5$		$Ra_o = 10^6$	
Mesh	v_{max}	x	v_{max}	x	v_{max}	x
40×40, 1:1	-0.342	0.950	-0.302	0.950	-0.255	0.950
60×60, 8:1	-0.404	0.965	-0.408	0.978	-0.390	0.984
80×80, 8:1	-0.408	0.970	-0.413	0.979	-0.398	0.988

TABLE 12 - Minimum Nodal Shear Stress Along (x, 0.0), $x \in (0, 1)$

	$Ra_o = 10^4$		$Ra_o = 10^5$		$Ra_o = 10^6$	
Mesh	$\partial v/\partial y\|_{min}$	x	$\partial v/\partial y\|_{min}$	x	$\partial v/\partial y\|_{min}$	x
40×40, 1:1	-0.0131	0.0250	-0.0742	0.975	-0.446	0.025
60×60, 8:1	7.11×10^{-3}	4.89×10^{-3}	-3.81×10^{-3}	0.0102	-0.0176	4.89×10^{-3}
80×80, 8:1	2.09×10^{-3}	0.0117	-4.91×10^{-3}	7.56×10^{-3}	4.69×10^{-4}	3.68×10^{-3}

TABLE 13 - Maximum Nodal Shear Stress Along (x, 0.0)

	$Ra_o = 10^4$		$Ra_o = 10^5$		$Ra_o = 10^6$	
Mesh	$\partial v/\partial y\|_{max}$	x	$\partial v/\partial y\|_{max}$	x	$\partial v/\partial y\|_{max}$	x
40×40, 1:1	-10.8	0.725	-11.4	0.775	-9.55	0.825
60×60, 8:1	-17.2	0.769	-35.0	0.949	-54.1	0.886
80×80, 8:1	-17.4	0.768	-36.4	0.838	-61.2	0.882

TABLE 14 - Computational Effort, $Ra_o = 10^4$

Mesh	N	Memory (Mbytes)	CPU Time (seconds)	Initial Condition
40×40, 1:1	1681	7.5	1,530	T= u= v= 0
60×60, 8:1	3721	15	5,100	T= u= v= 0
80×80, 8:1	6561	25	13,030	T= u= v= 0

TABLE 15 - Computational Effort, $Ra_o = 10^5$

Mesh	N	Memory (Mbytes)	CPU Time (seconds)	Initial Condition
40×40, 1:1	1681	7.5	1,430	$Ra_o = 10^4$
60×60, 8:1	3721	15	4,470	$Ra_o = 10^4$
80×80, 8:1	6561	25	8,540	$Ra_o = 10^4$

TABLE 16 - Computational Effort, $Ra_o = 10^6$

Mesh	N	Memory (Mbytes)	CPU Time (seconds)	Initial Condition
40×40, 1:1	1681	7.5	1,160	$Ra_o = 10^5$
60×60, 8:1	3721	15	6,550	$Ra_o = 10^5$
80×80, 8:1	6561	25	17,050	$Ra_o = 10^5$

FIGURES

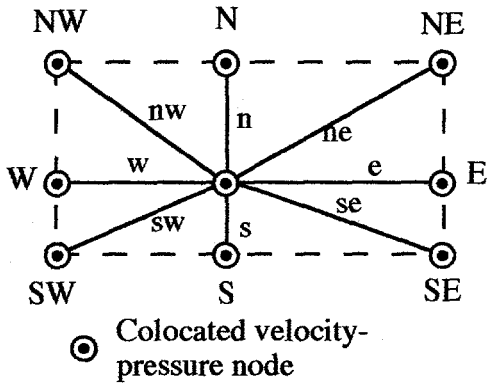

FIGURE 1 - Sample Eight Node Computational Molecule

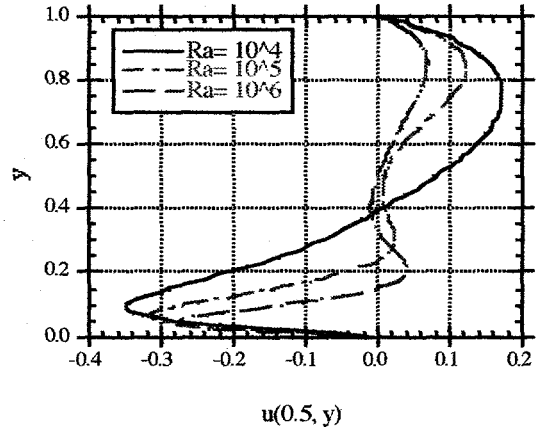

FIGURE 2 - u Velocity Component Variation Along Vertical Centerline

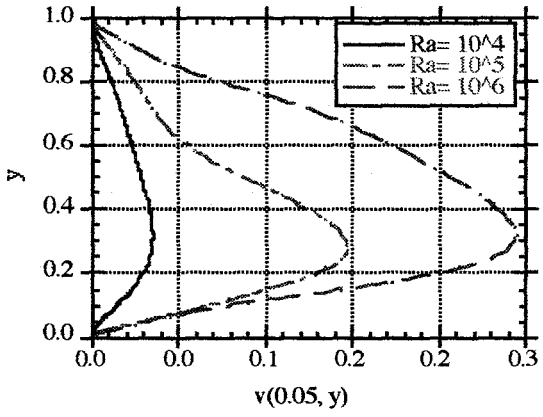

FIGURE 3 - v Velocity Component Variation Near Hot Wall

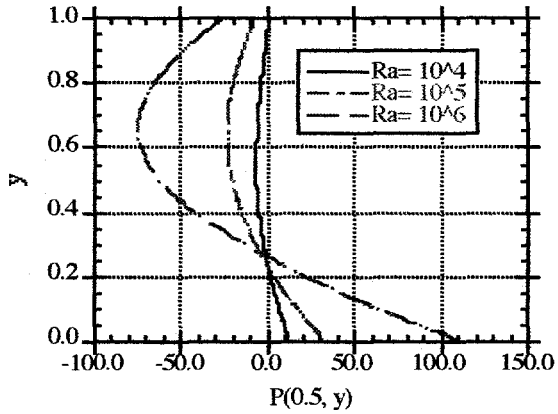

FIGURE 4 - Pressure Variation Along Vertical Centerline

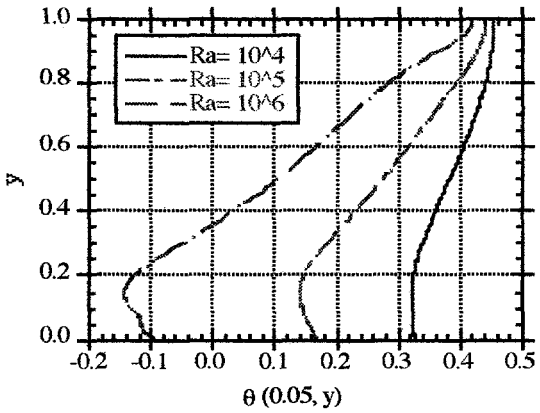

FIGURE 5 - Temperature Variation Near Hot Wall

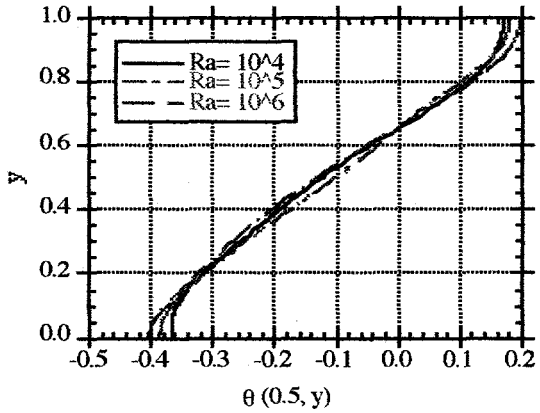

FIGURE 6 - Temperature Variation Along Vertical Centerline

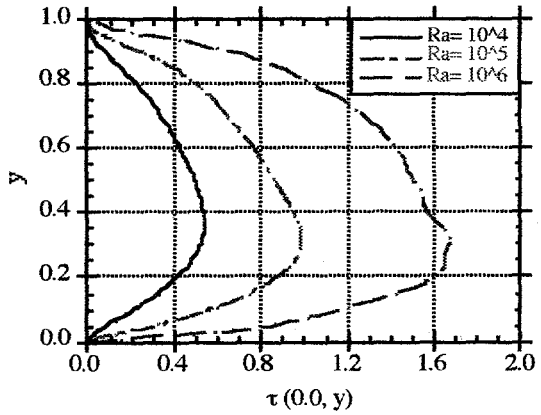

FIGURE 7 - Shear Stress Variation Along Hot Wall

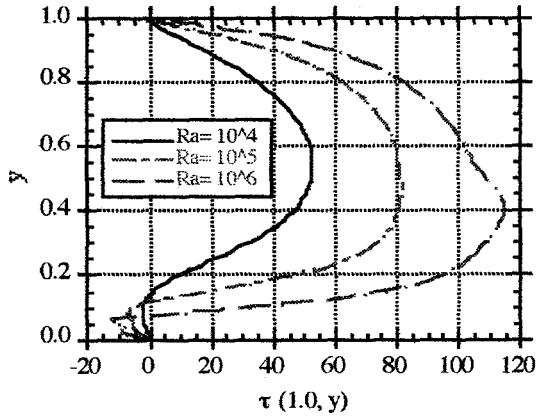

FIGURE 8 - Shear Stress Variation Along Cold Wall

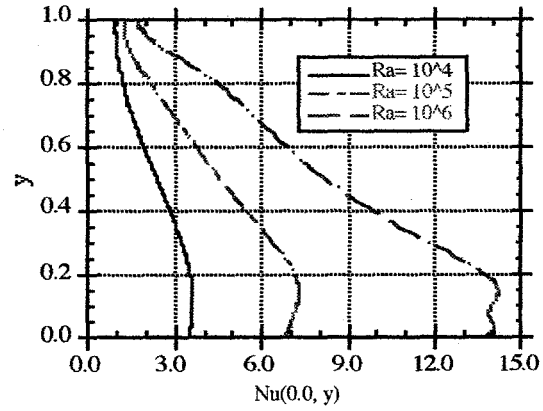

FIGURE 9 - Nusselt Number Variation Along Hot Wall

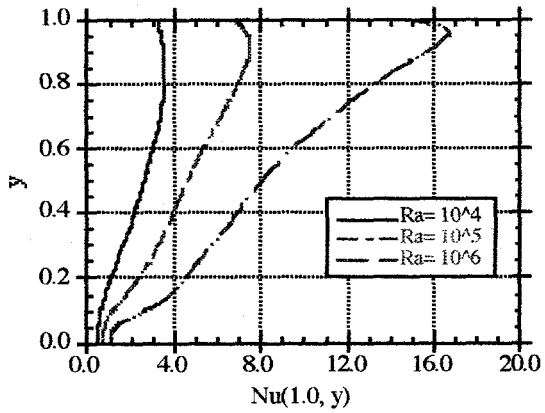

FIGURE 10 - Nusselt Number Variation Along Cold Wall

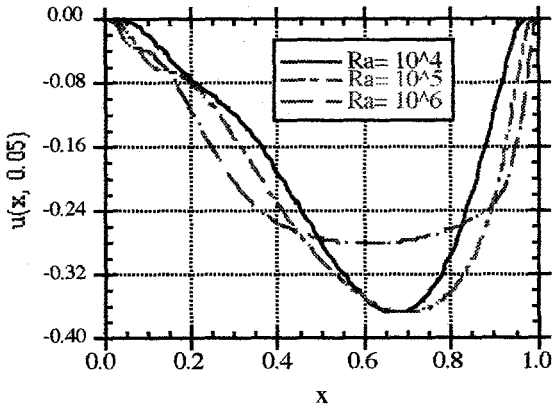

FIGURE 11 - u Velocity Component Variation Near Bottom Wall

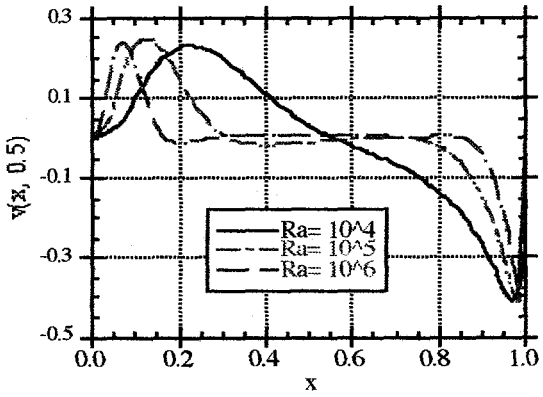

FIGURE 12 - v Velocity Component Variation Along Horizontal Centerline

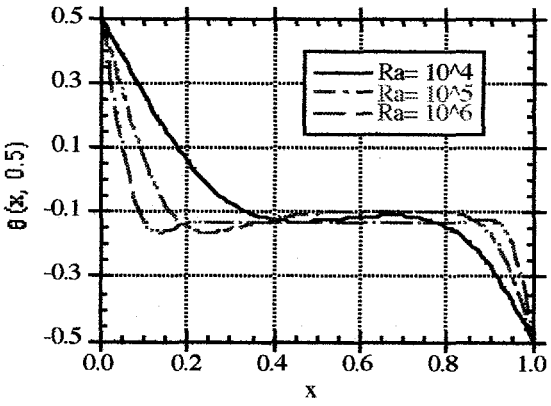

FIGURE 13 - Temperature Variation Along Horizontal Centerline